



Epstein–Barr virus and the immune microenvironment in multiple sclerosis: Insights from high-dimensional brain tissue imaging

Noga Orr^{a,1} and Lawrence Steinman^{a,b,1}

Affiliations are included on p. 11.

Contributed by Lawrence Steinman; received December 10, 2024; accepted January 23, 2025; reviewed by Howard Weiner and Hartmut Wekerle

Epstein–Barr virus (EBV) is strongly implicated in the pathogenesis of multiple sclerosis (MS), yet its exact role in disease progression remains unclear. Using high-dimensional CO-detection by indexing, a technology for spatial imaging, this study examines the cellular microenvironment of MS lesions in secondary progressive MS and primary progressive MS. We analyzed immune, glial, neuronal, and endothelial cell interactions within MS lesions and normal-appearing white matter across two independent cohorts. Our findings show the enrichment of EBV markers, particularly EBNA1 and LMP1, within MS lesions. EBV-positive cells interact closely with reactive astrocytes, microglia, and neurons. Image analysis confirmed the presence of EBV-positive staining within neurons and glial cells, suggesting a direct role for EBV in neuronal and glial involvement in MS. Additionally, we observed altered immune cell interactions, including reduced associations with macrophages and memory T cells, and enhanced interactions with glial cells. Disruptions in blood–brain barrier integrity were also noted in regions of the MS brain. These results highlight EBV's contribution to immune modulation, glial dysfunction, and neuronal damage in MS, particularly in progressive subtypes. The analysis of MS brain tissue suggests potential therapeutic targets, including antivirals and brain penetrant immune modulators, to address EBV's impact on MS progression.

Epstein–Barr virus | molecular mimicry | high-dimensional profiling | multiple sclerosis | tissue profiling

Epstein–Barr virus (EBV) is a ubiquitous virus, infecting over 90% of the global population and typically persisting in B cells in a latent state. Nearly all individuals with multiple sclerosis (MS) test positive for EBV, and its presence is particularly noted in MS brain lesions (1–6). This strong association suggests that EBV may play a pivotal role in the pathogenesis of MS, though the mechanisms by which EBV contributes to neuroinflammation and neurodegeneration remain under intense investigation.

Previous studies have shown the presence of EBV within MS lesions but lacked the spatial resolution and depth to examine the complex cellular interactions that might drive disease progression. In this study, we employed high-dimensional CO-detection by indexing (CODEX), a technological advance in spatial imaging to better understand EBV-related alterations in MS brain tissue. This powerful technique enabled the multiplexed analysis of up to 50 cellular markers in a single tissue sample, revealing the intricate interactions between immune, glial, endothelial, and neuronal cells in their native microenvironment. This approach provided the unique ability to simultaneously capture the cellular composition of MS lesions and the dynamic spatial relationships between EBV-infected cells and neighboring immune and central nervous system (CNS)-resident cells.

Using the AKOYA PhenoCycler-Fusion platform, we conducted highly detailed, spatially resolved analyses at single-cell resolution. This allowed us to map the relationships between EBV-infected cells and their surrounding immune and glial cells and assess the spatial proximity of viral markers (such as EBNA1 and LMP1) to critical tissue structures. Unlike traditional imaging methods, which could not often fully capture cellular proximity or marker colocalization, this imaging method provided a rich, multidimensional view of tissue architecture and cellular behavior. We examined cellular interactions within the MS lesion microenvironment, capturing subtle changes in immune dynamics linked to EBV infection and MS pathology.

This study analyzed brain tissue from two independent cohorts, focusing on secondary progressive MS (SPMS) and primary progressive MS (PPMS). We investigated EBV-related alterations in cellular interactions and spatial dynamics, aiming to better understand how EBV might influence immune activation, neuronal damage, and blood–brain barrier

Significance

This study demonstrates a widespread spatial impact of Epstein–Barr virus (EBV), which likely shapes the immune microenvironment within multiple sclerosis (MS) lesions. The spatial relationships with the resident glial cells and neurons within the central nervous system (CNS) may have significant implications for disease progression and for therapeutic countermeasures. Using high-dimensional CO-detection by indexing (CODEX) imaging, we found EBV-related markers enriched in MS lesions, particularly in progressive MS subtypes. These interactions may drive sustained inflammatory activity and disruption of the blood–brain barrier (BBB). This work underscores the importance of EBV as a major contributor to MS pathology, highlighting therapeutic targets such as antiviral strategies and immune modulators that could mitigate inflammation and neuronal damage within the CNS.

Author contributions: N.O. and L.S. designed research; N.O. performed research; N.O. and L.S. analyzed data; and N.O. and L.S. wrote the paper.

Reviewers: H. Weiner, Harvard University; and H. Wekerle, Max Planck Institute.

The authors declare no competing interest.

Copyright © 2025 the Author(s). Published by PNAS. This open access article is distributed under [Creative Commons Attribution-NonCommercial-NoDerivatives License 4.0 \(CC BY-NC-ND\)](https://creativecommons.org/licenses/by-nc-nd/4.0/).

¹To whom correspondence may be addressed. Email: ornoga@gmail.com or steiny@stanford.edu.

This article contains supporting information online at <https://www.pnas.org/lookup/suppl/doi:10.1073/pnas.2425670122/-/DCSupplemental>.

Published March 10, 2025.

(BBB) disruption in these MS subtypes. The high-dimensional data generated offered a comprehensive view of the cellular microenvironment in MS lesions, revealing potential therapeutic targets within the EBV-infected cellular landscape of the CNS.

Results

EBV Is Elevated and Alters Cellular Interactions in MS Lesions and Subtypes. Comparison of MS and non-MS samples revealed a significant increase in the frequency of EBV-related markers (e.g., EBNA1, EBNA2, LMP1) and disrupted cell–cell interactions, suggesting a perturbed cellular microenvironment in MS lesions. EBV-positive EBNA1 CD20 cells could be detected in MS brain samples (Fig. 1*A*). EBV marker frequency, particularly EBNA1, was notably elevated in MS lesions compared to non-MS controls ($P = 0.0086$, Fig. 1*B*), with EBNA2 and LMP1 also showing higher expression (*SI Appendix*, Fig. S1 *C* and *D*). We validated the specificity of staining for EBV markers using multiplexed-staining of human tonsil samples (*SI Appendix*, Fig. S1*A*) and cross-validated with in situ hybridization (ISH) of EBV-encoded RNA (EBER) both in tonsil and MS brain (*SI Appendix*, Fig. S1*B*). Importantly, we observed EBNA1 staining in and around the nucleus, with lower levels in the cytoplasm, a finding further confirmed by EBER-ISH, which also identified some EBV RNA in these compartments (7). Notably, the MS samples analyzed here include those characterized by Moreno et al., which demonstrated elevated EBV markers in MS brain tissue compared to controls (7). These findings build on and extend earlier observations (7) by incorporating spatially resolved analysis of EBV-positive cells and their interactions within the lesion microenvironment.

Cell–cell interactions were analyzed using two complementary methods: log odds ratios and Euclidean distances. Log odds ratios, as described by Goltsev et al. (8), quantify the likelihood of interactions between specific cell types by comparing their observed co-occurrence in MS lesions to control samples. Positive values indicate increased interaction likelihood, while negative values suggest decreased likelihood.

In contrast, Euclidean distances focus on the spatial proximity between cells, computed using the Spatial Neighbor Distance extension. For each cell of a given “from” type, the algorithm identifies the nearest neighbor of a specified “to” type and measures the direct spatial distance (d). This approach highlights shifts in cellular organization and physical proximity, providing a spatial perspective on cell–cell relationships that complement the probabilistic insights from log odds ratios (*Materials and Methods*).

Astrocytes in MS lesions were more likely to interact with EBNA1+ and LMP1+ cells (log₂ odds ratio: EBNA1 = 0.48, $P = 0.005$; LMP1 = 0.36, $P = 0.02$) (Fig. 1 *C* and *D*). Increased associations were also observed between EBNA1+ and LMP1+ cells and GlialCaM-expressing astrocytes (*SI Appendix*, Fig. S1 *D* and *E*). We had a particular interest in GlialCAM, having described molecular mimicry between GlialCAM and EBNA-1 in a study of clonal antibodies found in the CSF of individuals with MS (2).

EBV-positive cells showed enhanced interaction odds with neurons (EBNA1 = 0.45, $P = 0.01$; LMP1 = 0.46, $P = 0.04$) (Fig. 1 *E* and *F*) but reduced odds with activated macrophages (CD14+IBA1-CD68+; -0.37 , $P = 0.04$) and memory T cells (CD45RO+CD3e+; 0.45, $P = 0.01$) (*SI Appendix*, Fig. S1 *G* and *H*).

Euclidean distance analysis showed that EBNA1+ cells were closer to neurons ($P = 0.03$) and EBNA2+ cells were closer to GFAP+GlialCaM+ astrocytes in MS lesions compared to non-MS controls ($P = 0.044$) (Fig. 2*A*). EBNA1+ cells were spatially closer to OLIG2+ oligodendrocytes, microglia, and

neurons, reflecting interactions with key glial and neuronal populations in MS lesions.

Building on these spatial proximity findings, image analysis confirmed EBNA1 staining within astrocytes, microglia, and neurons, providing direct evidence of EBV infection in glial and neuronal cells in MS tissues (Fig. 2 *B–D*). These findings support a link between EBV and both glial and neuronal involvement in the EBV-infected CNS in MS.

Our cohort included SPMS and PPMS patients, enabling the analysis of subtype-specific differences in cellular interactions and the role of EBV in spatial dynamics. Frequency analysis showed significantly higher astrocyte density in PPMS lesions ($P = 0.016$) (Fig. 3*F*), while SPMS lesions exhibited increased M2 microglia (IBA1+CD163+; $P = 0.05$) (Fig. 3*G*).

In PPMS, M2 microglia showed significantly higher odds of interacting with EBNA1+ and LMP1+ cells (Fig. 1 *G* and *H*), as well as with memory T cells and GlialCaM+AQP4+ astrocytes (*SI Appendix*, Fig. S4 *F* and *G*). Euclidean distance analysis corroborated these findings, highlighting spatial differences in cell–cell relationships between subtypes (*SI Appendix*, Fig. S4*H*). Additionally, EBNA1+ and EBNA2+ cells in PPMS were found to be closer to MAP2+NeuN+ neurons, emphasizing EBV's role in subtype-specific spatial interactions within the MS lesion microenvironment.

Hence, EBV-related markers were elevated in MS lesions and were associated with altered cellular interactions and spatial dynamics. Notably, EBV infection of neurons was confirmed through EBNA1 staining, providing direct evidence of neuronal involvement in MS. EBV-positive cells exhibited enhanced interactions with astrocytes and neurons while showing reduced interactions with macrophages and memory T cells. Subtype-specific differences highlighted increased astrocyte density in PPMS and a greater association of M2 microglia with EBV-positive cells, emphasizing the distinct roles of EBV in the MS microenvironment.

Reactive Glial-Neuronal Interactions Reveal Pathological Changes in the Microenvironment of MS Lesions.

CODEX multiplexed imaging revealed detailed brain structures and glial–neuronal interactions, with progressively magnified views illustrating the spatial relationships and cellular organization in MS samples (*SI Appendix*, Figs. S2 and S3). Thereby, enabling the identification of disruptions in the glial–neuronal microenvironment in MS lesions. These disruptions included increased NeuN staining and decreased MAP2 staining, indicative of neuronal loss (Fig. 3*A*). This was also evident by the decreased frequency of neurofilament in MS samples (*SI Appendix*, Fig. S4*A*). Macrophages and microglia were reduced in central lesion regions but accumulated at the borders, with these patterns and neuronal loss more pronounced in PPMS compared to SPMS. An increase in GFAP+ astrocytes and IBA1+ microglia relative to AQP4+ astrocytes was observed in MS compared to non-MS controls, suggesting a transition to chronic lesion states (Fig. 3*B*). Accordingly, interactions between neurons and AQP4+ astrocytes within lesions were elevated (*SI Appendix*, Fig. S4*B*).

Log odds ratio analysis revealed enhanced interactions between neurons and reactive glial cells, including GlialCaM+ astrocytes and activated microglia (GFAP+GlialCaM+; 0.58, $P = 0.024$, IBA1+CD68+HLA-DR+; 0.33, $P = 0.027$) (Fig. 3 *C* and *D*). Oligodendrocytes showed increased interactions with activated microglia (log odds = 0.39, $P = 0.015$) (Fig. 3*E*).

Euclidean distance analysis further revealed demyelination, with greater distances between MBP+ oligodendrocytes and neurons in MS lesions ($P = 0.00012$), and closer proximity of microglia and neurons ($P = 0.001$, Fig. 2*A*).

In PPMS, reduced cellularity and increased gliosis were observed compared to SPMS (Fig. 3 *A* and *F*), with shorter Euclidean

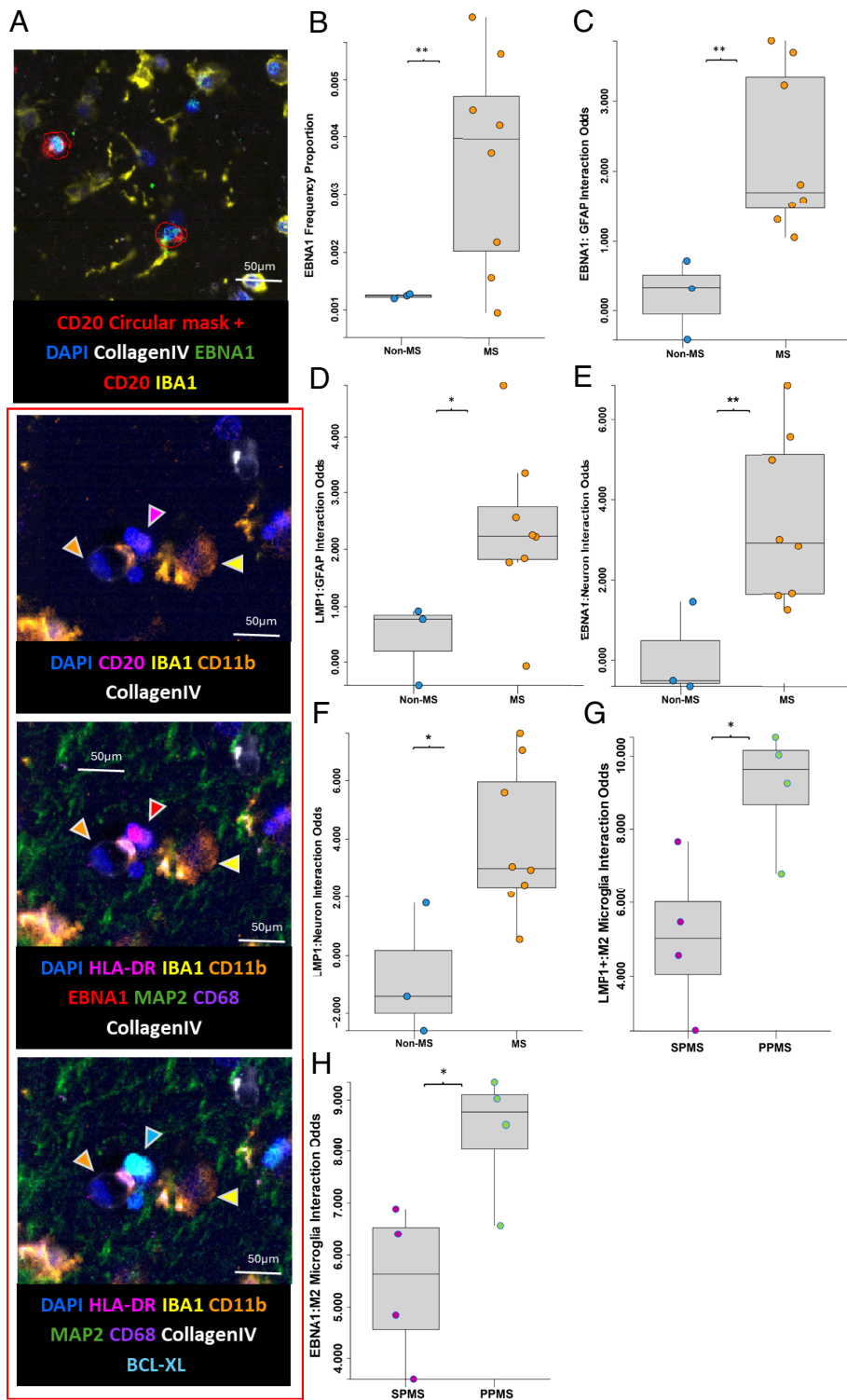


Fig. 1. EBV-related changes and interactions in MS lesions. (A) Representative images of EBV-positive CD20⁺ cells in MS brain tissue. (Top) CD20⁺ gating mask (circular red line) confirmed by staining. (Bottom) Representative image of EBNA1+CD20⁺ B cell expressing BCL-XL antiapoptotic marker interacting with activated microglia and macrophage. Series of images of the same cells (3 panels in red box): (Top) CD20⁺ (pink arrow), (Middle) EBNA1⁺ (red arrow), (Bottom) BCL-XL⁺. (B) EBNA1 marker frequency is higher in MS lesions compared to non-MS controls (mean difference = 0.46, $P = 0.0086$). Log odds ratio analysis indicates significantly increased interactions between EBNA1⁺ or LMP1⁺ cells and reactive astrocytes ($P = 0.0048$ and $P = 0.02$, respectively; log odds: EBNA1 = 0.48, LMP1 = 0.36) (Panels C and D). Similarly, EBNA1⁺ and LMP1⁺ cells exhibit enhanced interactions with neurons ($P = 0.01$ and $P = 0.04$, respectively; log odds: EBNA1 = 0.45, LMP1 = 0.46) (Panels E and F). Analysis of interaction odds ratios further reveals that M2 microglia are more frequently associated with EBNA1⁺ and LMP1⁺ cells ($P = 0.009$ and $P = 0.015$, respectively; log odds: EBNA1 = 0.56, LMP1 = 0.52), while GlialCaM+AQP4⁺ astrocytes in PPMS lesions also demonstrate an increased association (log odds = 0.48, $P = 0.02$) (Panels G and H).

distances between astrocytes, activated macrophages ($P = 0.06$), and neurons.

These findings highlight disrupted glial–neuronal interactions in MS lesions, with enhanced microglial–neuronal interactions and increased astrocytic reactivity, reflecting an altered micro environment.

Immune Cell Enrichment and Increased Proximity to Glial and Neuronal Cells in MS. Immune cells play a central role in MS pathology, where their infiltration and interactions with glial and neuronal cells drive inflammation and neurodegeneration.

High-resolution spatial analysis identified distinct immune cell patterns and interactions within the lesion microenvironment. In addition to the increased numbers of EBV-positive cells described above, we found an enrichment of B cells, T cells, macrophages, and activated microglia in MS lesions compared to non-MS controls (Fig. 4A and B). Analysis of lesions vs. normal-appearing white matter (NAWM) showed immune cell infiltration into the lesion area. In contrast, in NAWM, immune cells were primarily located in or around the vasculature (SI Appendix, Fig. S4E).

Elevated interaction odds were observed between neurons and various immune cell subsets, including CD138⁺ plasma cells,

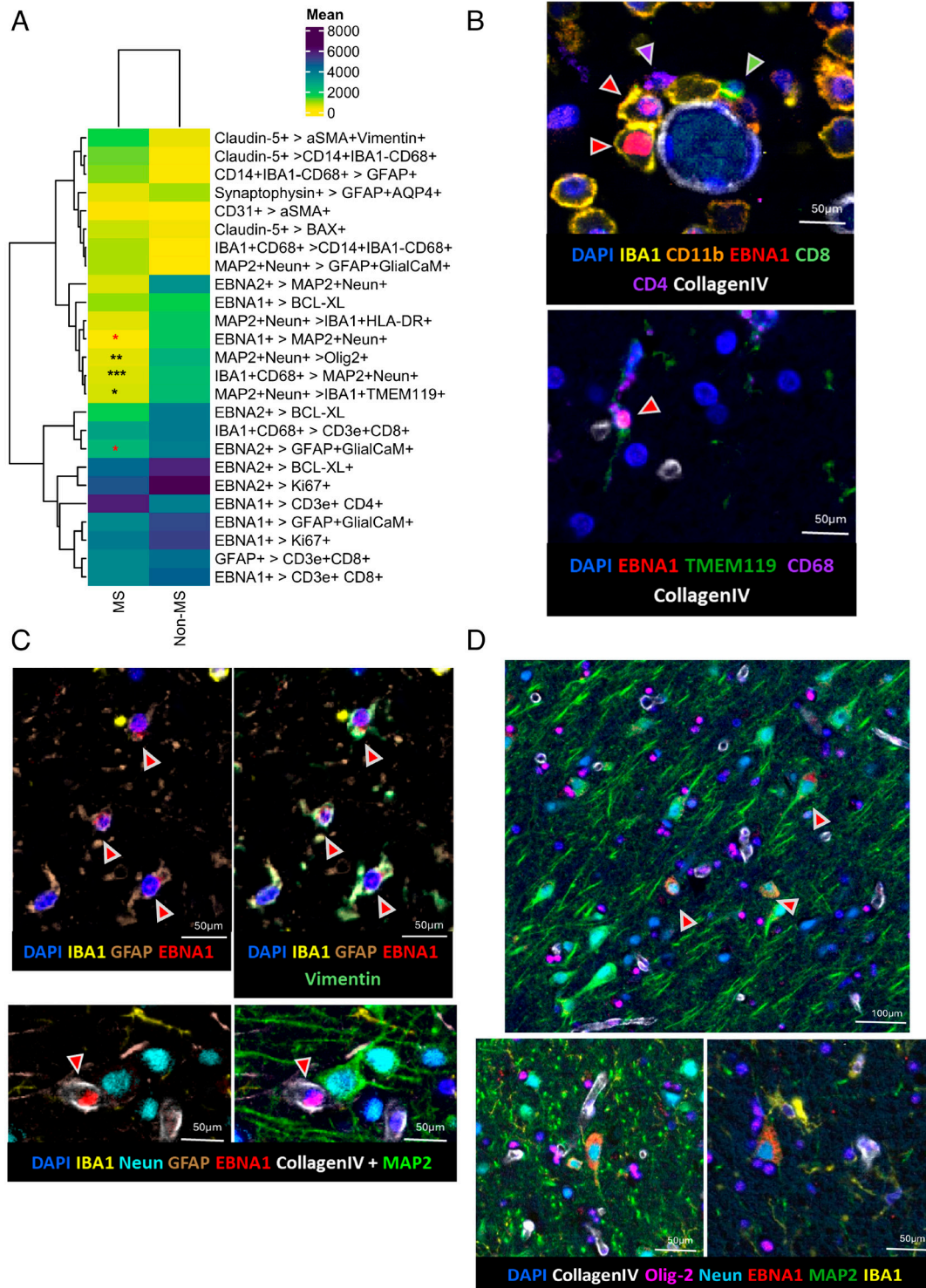


Fig. 2. Euclidian cell-distance and EBNA1⁺ positive neurons and glial cells in MS lesions. (A) Heatmap of Euclidean distance analysis comparing cell proximity in MS vs. non-MS. Significant findings (depicted by asterisks) EBNA1⁺MAP2+Neun+ ($P = 0.03$), EBNA2⁺GFAP+GlialCaM+ ($P = 0.044$), MAP2+Neun+ Olig2+ ($P = 0.00012$), IBA1+CD68+MAP2+Neun+ ($P = 0.001$). Immunofluorescence shows EBNA1 localization (red arrows) within. (B) Microglia: (Top) EBNA1⁺ microglia (red arrows) interacting with T cells (CD4⁺ purple arrow, CD8⁺ Green arrow) and activated macrophage (orange). (Bottom) EBNA1⁺TMEM119⁺ microglia. (C) Astrocytes: (Top) EBNA1 is found in GFAP+Vimentin+ Astrocytes; both panels show the same area in the MS brain. (Bottom) EBNA1 is found in astrocyte interacting with neuron soma; both panels show the same area in the brain. (D) Neurons: (Top) Representative image of 100 μm field of view depicting EBNA1⁺ and EBNA1⁻ neurons. (Bottom) Left depicts EBNA1⁺ neurons; right depicts EBNA1⁺ neurons interacting with IBA1⁺ microglia (yellow).

CD45RO⁺ memory T cells, CD4+CD8⁺ double-positive T cells (Fig. 4 C–E), and HLA-DR⁺ antigen-presenting microglia (Fig. 3D) (CD138⁺; 0.38, $P = 0.034$, CD3e+CD45RO⁺; 0.45, $P = 0.025$, CD4+CD8⁺; 0.47, $P = 0.022$, IBA1+CD68+HLA-DR⁺; 0.33, $P = 0.027$). Oligodendrocytes also showed increased interaction odds with macrophages and activated microglia (CD14+

CD11b+CD68⁺; 0.26, $P = 0.05$; IBA1+CD68⁺; 0.39, $P = 0.01$) (Fig. 5 A and B). An interaction between Vimentin⁺ smooth muscle cells and CD45RO⁺ memory T cells was also noted (log odds = 0.38, $P = 0.049$) (SI Appendix, Fig. S4C).

Euclidean spatial analysis confirmed increased immune–neuronal interactions in MS lesions. Activated and homeostatic microglia were

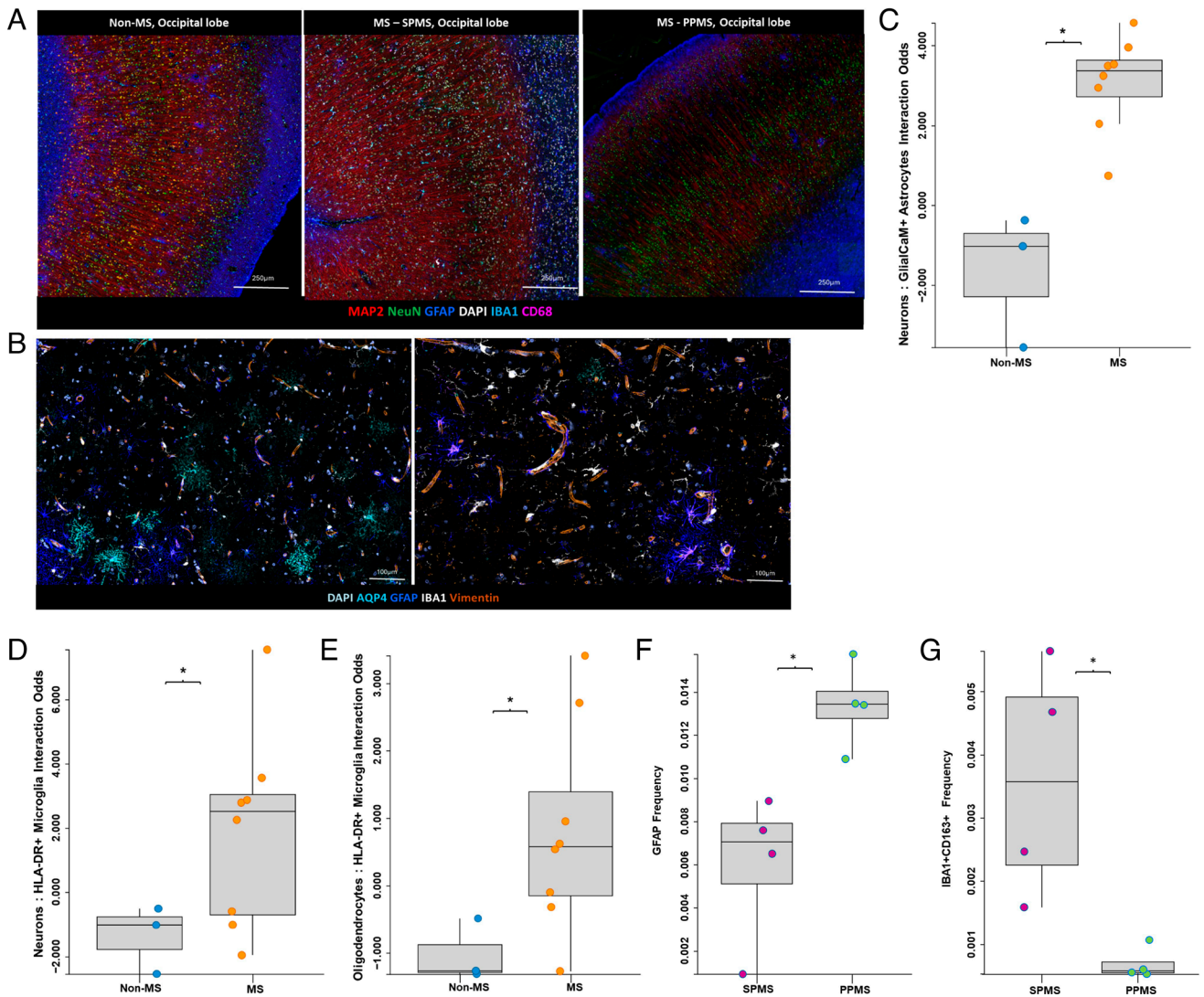


Fig. 3. Glial-neuronal interactions and gliosis in MS lesions. (A) Representative multiplexed immunofluorescence images showing neuronal loss in MS brain samples, analyzed using PhenoCycler Fusion. (B) Representative multiplexed immunofluorescence images, showing increased GFAP+ astrocytes (blue) and IBA1+ microglia (white) relative to AQP4+ astrocytes (aqua) in MS samples. (C–E) Log₂ odds ratio analysis in non-MS vs. MS brain samples. (F and G) Frequency analysis of GFAP+ astrocytes (F) and IBA1+CD163+ microglial cells (G) in SPMS vs. PPMS brain samples.

positioned closer to neurons and oligodendrocytes. CD4+ and CD8+ T cells were also located closer to neurons and astrocytes. MBP+ oligodendrocytes were closer to CD14+ macrophages (Fig. 2A).

Image analysis confirmed a marked increase in immune cell presence in SPMS, with clustering around perivascular cuffs throughout the lesion areas. In PPMS, immune cells were less abundant (Fig. 5C). SPMS lesions exhibited significantly higher frequencies of CD163+ M2 macrophages ($P = 0.05$) (Fig. 3G). Log odds ratio analysis revealed enhanced interactions between CD163+ M2 microglia and CD20+ B cells ($P = 0.016$), CD45RO+ memory T cells ($P = 0.019$), and activated astrocytes ($P = 0.027$) (SI Appendix, Fig. S4 D–F). Euclidean distance analysis further supported these findings, showing that GFAP+ astrocytes were positioned closer to activated macrophages in SPMS, highlighting increased immune activity and reactive gliosis. These findings were supported by Euclidean distance analysis, which demonstrates that GFAP+ astrocytes are positioned closer to activated macrophages in SPMS, highlighting the increased immune activity and reactive gliosis characteristic of this subtype (SI Appendix, Fig. S4H).

The results demonstrate increased immune cell frequency and enhanced interactions with glial and neuronal cells in MS lesions.

Closer proximity of T cells, microglia, and macrophages to neurons and oligodendrocytes suggests immune-driven neurodegeneration. SPMS lesions showed heightened immune activity with higher T cell and macrophage frequencies and astrocytes positioned closer to activated macrophages, highlighting subtype-specific immune dynamics.

Compromised BBB Integrity and Structural Disruptions in MS Lesions. The BBB is essential for maintaining CNS homeostasis by regulating the exchange of molecules and cells between the bloodstream and the brain. In MS, BBB disruption allows immune cell infiltration and inflammation, contributing to lesion development and neurodegeneration. Our analysis revealed significant BBB integrity disruptions, altered spatial relationships, reduced cellular interactions, and structural remodeling within MS lesions.

Image analysis revealed a loss of Claudin-5+ and α -SMA+ cells, along with disrupted CD31+ endothelial cell continuity and elevated Bcl-2-associated X protein (BAX) expression, a pro-apoptotic protein that plays a crucial role in programmed cell death, in perivascular cuffs within MS lesion areas compared to non-MS controls (Fig. 6A). A comparison of CD31+

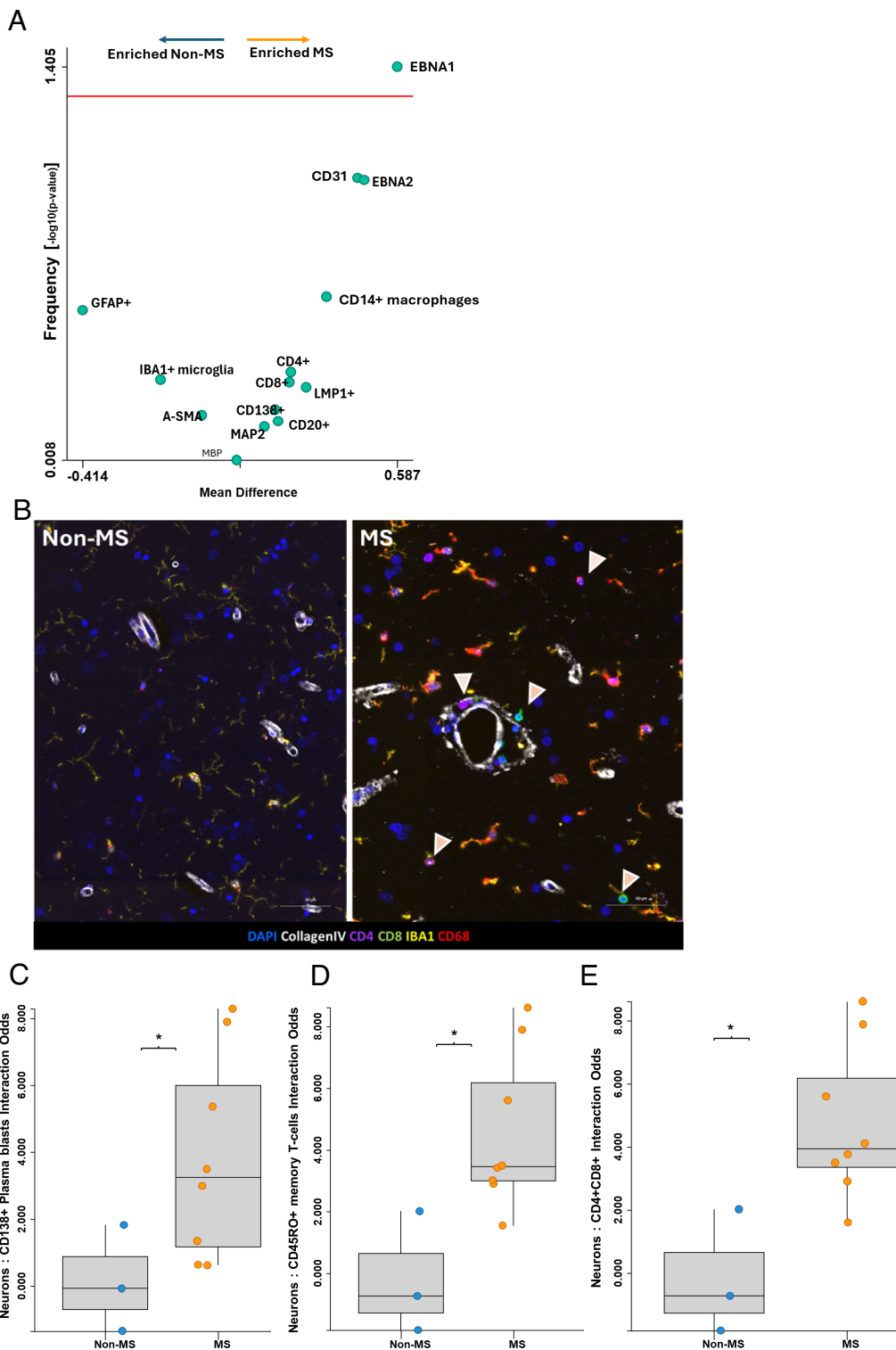


Fig. 4. Immune cell enrichment and interactions in MS lesions. (A) Volcano plot showing frequency enrichment of immune cells in MS lesions compared to non-MS controls. (B) Representative multiplexed immunofluorescence images showing immune cell infiltration in MS lesions (*Right*) compared to non-MS control tissue (*Left*). Immune cells such as CD4+ T cells, CD8+ T cells, IBA1+ microglia, and CD68+ macrophages are enriched in MS lesions. (Scale bar: 200 μ m.) (C–E) Log2 odds ratio analysis showing enhanced interactions between neurons (MAP2) and various immune cells, including CD4+CD8+ double-positive T cells (log odds = 0.47, P = 0.022), CD45RO+ memory T cells (log odds = 0.45, P = 0.025), IBA1+CD68+HLA-DR+ antigen-presenting microglia (log odds = 0.33, P = 0.027), and CD138+ plasma cells (log odds = 0.38, P = 0.034).

endothelial cell frequency showed a significant reduction in lesions compared to NAWM within the same sample (P = 0.036) (Fig. 6*B*).

The log-odds ratio analysis showed reduced interactions between Claudin-5+ BBB endothelial cells and various cellular components in

MS lesions compared to non-MS controls. These included diminished interactions with Vimentin+ pericytes (log odds = -0.48 , P = 0.006), Synaptophysin+ synaptic neurons (log odds = -0.49 , P = 0.007), CD68+ activated macrophages (log odds = -0.39 , P = 0.014) (Fig. 6 C–E). Reduced interaction odds were also observed with EBNA2+

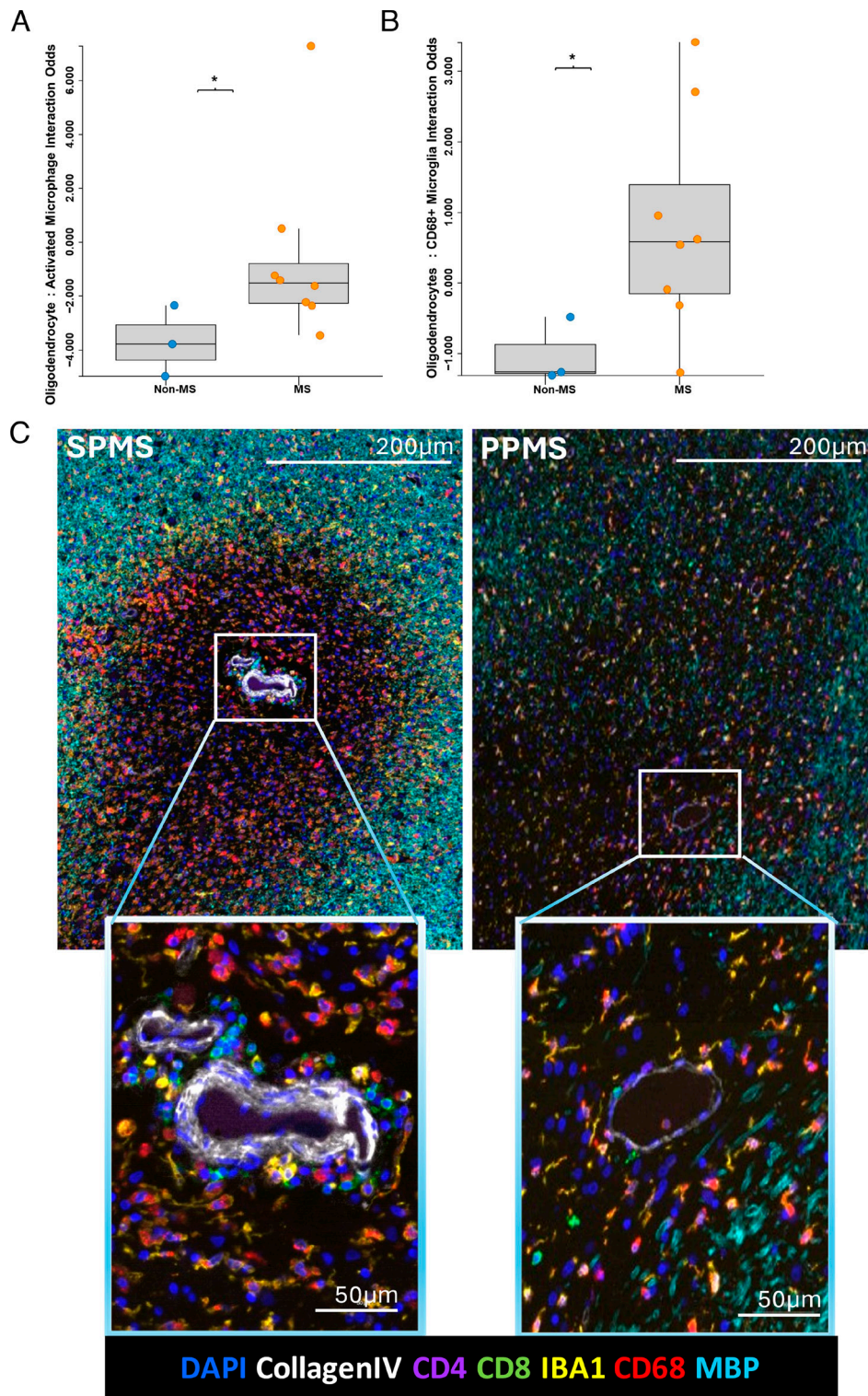


Fig. 5. Immune cell enrichment and interactions in SPMS vs. PPMS lesions. (A and B) Log₂ odds ratio analysis showing increased interactions between oligodendrocytes (MBP) and activated microglia (IBA1+CD68+) and macrophages (CD14+CD11b+CD68+) in MS lesions (CD14+CD11b+CD68+; log odds = 0.26, $P = 0.05$; IBA1+CD68+; log odds = 0.39, $P = 0.01$). (C) Representative multiplexed immunofluorescence images showing immune cell clustering around perivascular cuffs throughout SPMS lesion areas (Left) compared to PPMS lesions (Right), where immune cell presence is less abundant. Top panels: Lesion areas at low magnification (200 µm). Bottom panels: High magnification (50 µm) of the same regions, focusing on the perivascular areas where immune cells are clustered.

cells (log odds = -0.39 , $P = 0.022$), EBNA1+ cells (log odds = -0.36 , $P = 0.029$) (Fig. 6 F and G), and CD45RO+ memory T cells (log odds = -0.35 , $P = 0.050$) (SI Appendix, Fig. S4D).

In contrast, in non-MS samples, Claudin-5 was predicted to be closer to T cells, B cells, and activated macrophages, indicating that the BBB in these patients was intact, confining immune cells

to areas enveloped within the BBB. Moreover, EBV markers in non-MS samples showed limited interactions with neuronal populations, consistent with an intact barrier.

In SPMS, Euclidean distance showed that Claudin-5+ BBB endothelial cells were closer to Glut-1+ astrocytes (398.56 µm in SPMS vs. 783.99 µm in PPMS) (SI Appendix, Fig. S4H), and

CD31+ endothelial cell expression was less continuous than in PPMS, indicating compromised BBB integrity. Spatial relationships between endothelial cells and structural markers, such as

smooth muscle cells and astrocytes, also showed subtle changes, particularly in SPMS, further reflecting compromised BBB integrity.

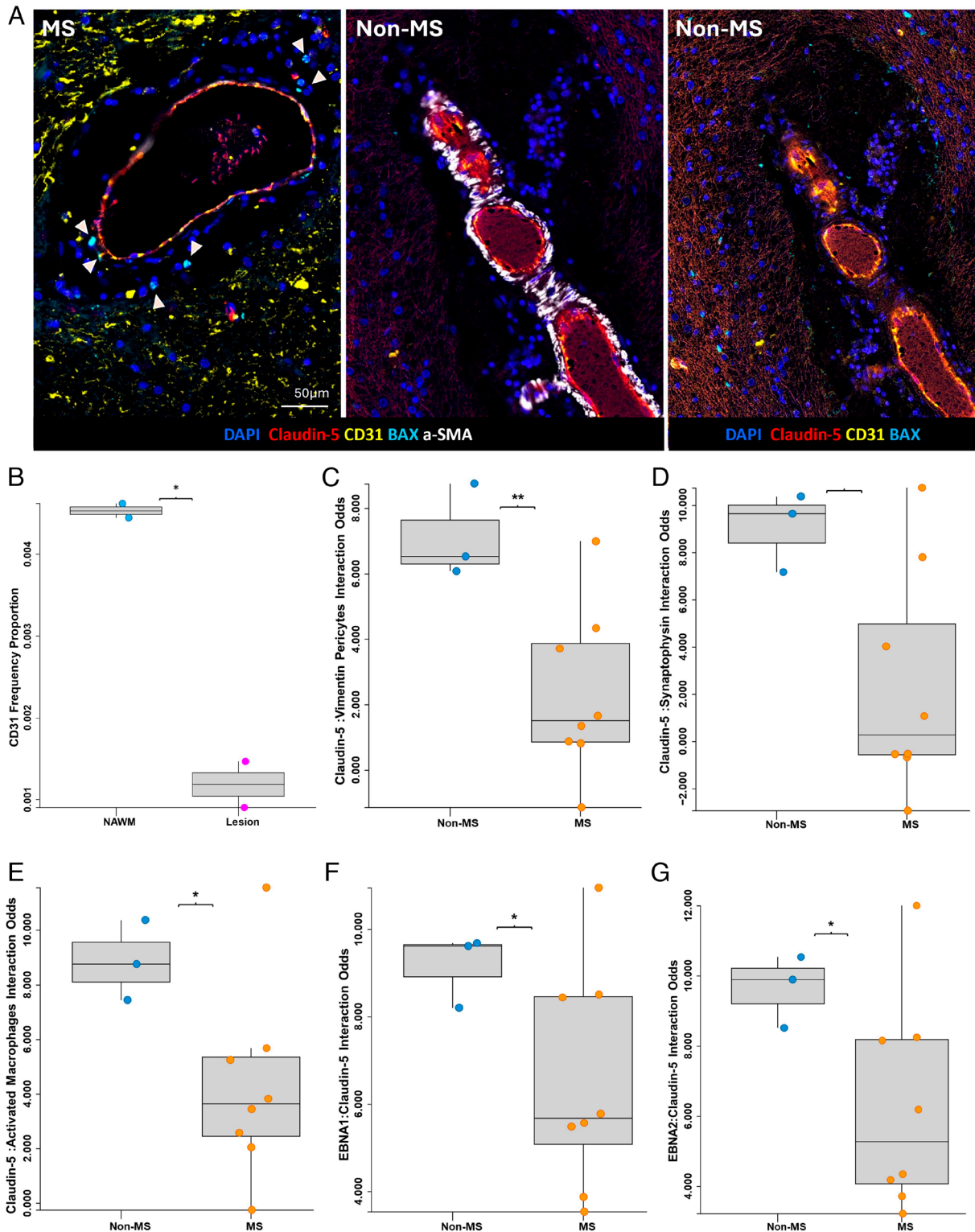


Fig. 6. Disruption of BBB integrity in MS lesions. (A) Representative multiplexed immunofluorescence images showing changes in BBB markers in MS lesions (Left) and non-MS controls (Right). The images show Claudin-5 (red) and CD31 (yellow) expression in relation to the perivascular area, with increased BAX (aqua, marked by arrows) expression indicating endothelial apoptosis in MS lesions. (Scale bar: 200 μm.) (B) Frequency analysis of CD31+ endothelial cells in MS lesions compared to NAWM from the same samples, with significant differences observed (mean difference = -0.9, $P = 0.036$). (C–E) Log2 odds ratio analysis showing reduced associations of Claudin-5+ endothelial cells with Vimentin+ pericytes (log odds = -0.48, $P = 0.039$), Synaptophysin+ synaptic neurons (log odds = -0.49, $P = 0.0073$), and CD68+ activated macrophages (log odds = -0.39, $P = 0.0143$) in MS lesions compared to non-MS controls. (F and G) Log2 odds ratio analysis of diminished interactions between Claudin-5+ endothelial cells and EBNA1+ (log odds = -0.5, $P = 0.0024$) and EBNA2+ (log odds = -0.57, $P = 0.00054$) cells in MS lesions compared to non-MS controls.

These findings indicate compromised BBB integrity in MS lesions, with structural disruptions in the endothelial cell layer and altered vascular relationships, highlighting impaired barrier function.

Discussion

This high-dimensional application of CODEX technology to MS brain specimens taken at autopsy reveals that EBV markers, particularly EBNA1 and LMP1, are enriched in MS lesions compared to NAWM and healthy controls. These markers occur more frequently in lesions and are spatially closer to immune cells such as CD8+ T cells and IBA1+ microglia, indicating localized immune activation driven by EBV within MS lesions. This interaction between EBV-positive cells and immune cells is particularly pronounced in progressive MS subtypes, such as SPMS, where sustained inflammation may contribute to disease progression and tissue damage.

The differences in cellular composition and interactions between SPMS and PPMS provide insights into the divergent pathological mechanisms underlying these subtypes. In SPMS, heightened immune activity and an increased frequency of M2 microglia, which are generally associated with immune mediators thought to be “anti-inflammatory” and/or “immune regulatory” (9), suggest a central role for sustained immune responses in lesion progression. In contrast, PPMS lesions exhibit a prominence of astrocytes, with localized interactions between EBV-positive cells, microglia, astrocytes, and neurons. The proximity of EBV-positive cells to neurons in PPMS is striking, suggesting that EBV may directly contribute to neuronal stress or damage. This localized inflammatory response, possibly driven by EBV or through direct viral effects on neurons, points to EBV as a key factor in subtype-specific MS pathology.

Notably, the EBNA1 staining observed in MS lesions shows increased signal in the nuclei but also notable staining in the cytoplasm across multiple cell types, including neurons and glial cells. This cytoplasmic localization aligns with findings by Leung et al. (10), suggesting that EBNA1’s nuclear exclusion may enhance antigen presentation via macroautophagy, thereby facilitating immune recognition. While EBNA1 is typically nuclear, specific conditions, such as altered phosphorylation at serine 393, can lead to its relocalization to the cytoplasm (11). These observations highlight the dynamic subcellular localization of EBNA1 and suggest that EBV may employ distinct mechanisms to persist within various CNS-resident cell types, potentially contributing to cellular stress, immune activation, and the broader pathogenesis of MS. However, given the modest cohort size, caution is warranted in generalizing these findings, and further studies with larger datasets are needed to confirm these subtype-specific patterns and their implications for disease progression.

Our findings broaden the results of Moreno et al. (7) that showed a higher prevalence of EBV markers LMP1 and BZLF1 in B cells (CD20) and plasma cells (CD138) in MS cortical samples than controls. This study builds on those findings by utilizing the same specimens and subjecting them to single-cell and spatial profiling with the AKOYA PhenoCycler-Fusion platform. It offers a more detailed examination of EBV-positive cell types and their spatial relationships with surrounding immune and glial cells. This approach not only confirms our previous observations (7) but also provides deeper insight into the interactions between EBV-positive cells and the surrounding microenvironment.

Examination of lesions revealed a shift from the homeostatic glial–neuronal connectivity observed in NAWM, where neurons and synapses are closely associated with oligodendrocytes, to a

reactive microenvironment in lesions. Increased interactions between AQP4+ astrocytes, synaptophysin, and Claudin-5, alongside the prevalence of Vimentin+ and GlialCaM+ astrocytes, highlight the disruption of glial–neuronal interactions. The increased interactions suggest a shift to a more reparative environment, with nevertheless some continued inflammation. These findings underscore the critical role of reactive astrocytes in shaping the lesion microenvironment and their potential to disrupt normal glial–neuronal interactions, thereby contributing to MS pathology. The role of EBV in driving neuroinflammation and tissue damage in MS is further supported by findings from Hassani et al. (12), which demonstrated the presence of EBV in 90% of MS cases compared to only 24% of non-MS controls. In their study, EBV was found to infect not only B cells but also astrocytes and microglia, which is consistent with our observations of EBV-positive cells near glial and neuronal populations. These findings reinforce the idea that EBV plays a multifaceted role in shaping the immune microenvironment and promoting inflammatory cascades in MS lesions.

A potentially important observation in our study is the presence of EBNA1-positive neurons, suggesting latent EBV infection or an immune-mediated bystander effect within neurons in MS lesions. EBNA1-positive microglia and astrocytes were also detected. This is consistent with *in vitro* studies showing that EBV can infect human neuronal cells (13) and astrocytes (14), with evidence that EBV induces both latent and lytic cycles in neuronal cells and supports persistent infections in astrocytes. Additionally, Biebl et al. (15) described EBV-associated encephalitis, demonstrating the virus’s ability to directly infect neurons and glial cells, leading to extensive reactive astrogliosis, microgliosis, and lymphocytic infiltration—features also observed in MS lesions. These findings highlight the role of EBV in initiating localized inflammation and immune-mediated CNS damage, contributing to the neuroinflammatory cascades and tissue damage characteristic of MS.

Tiwari et al. (16) emphasized that EBV may contribute to MS pathogenesis through mechanisms such as oxidative stress and cell cycle dysregulation. In our study, the presence of EBV markers in close proximity to neurons highlights its potential neurotropic effects, suggesting a direct role in promoting neuronal stress and damage in MS. These findings underscore the importance of investigating EBV’s involvement in neuronal instability as a contributing factor to MS pathophysiology.

The concept of molecular mimicry, as described by Soldan and Lieberman (1), provides a mechanism by which EBV infection could lead to CNS-targeted autoimmunity. Recent work by Lanz et al. (2) identified a shared epitope between EBNA1 and GlialCAM, an adhesion molecule expressed on astrocytes and oligodendrocytes. This mimicry may trigger immune responses targeting both EBV-infected and CNS-resident cells, supporting a model of EBV-induced autoimmunity within the CNS. Our findings of EBV-positive cells in proximity to MAP2+NeuN+ neurons and GFAP+ astrocytes align with this mechanism, suggesting that EBV-positive cells in MS lesions contribute to neuroinflammation and glial activation through bystander effects.

Recent studies further highlight the role of EBV in immune evasion within the MS brain. Aloisi and Salvetti (3) demonstrated that EBV-infected B cells in MS brain tissue express PD-L1, which interacts with PD-1 on CD8+ and CD4+ T cells, potentially allowing infected cells to evade immune-mediated clearance. This mechanism of immune checkpoint-mediated evasion may explain the persistence of EBV in MS lesions, contributing to sustained inflammation and lesion formation. Our findings of EBV-positive cells adjacent to immune cells within MS lesions suggest that EBV may

evade immune responses while simultaneously promoting a proinflammatory environment. Similarly, Serafini et al. (17) emphasized that PD-L1 expression by EBV-infected cells could lead to T cell exhaustion, fostering chronic immune dysfunction within the CNS. This persistence of EBV, coupled with immune checkpoint-mediated evasion, may create an environment of chronic inflammation, impairing the immune system's ability to clear infected cells. A notable checkpoint inhibitor, alpha B Crystallin (CRYAB) (18–21) has been described contiguous to a region in EBNA-1 containing a molecular mimic to GlialCAM. The side-by-side appearance of molecular mimics to GlialCAM (2, 21) and CRYAB (17, 20, 21) in neighboring linear sequences of EBNA-1 is notable.

Though this study is on autopsy material and includes individuals in the progressive phases of the disease, the concept that early MS and the progressive forms of disease represent distinct aspects of MS where inflammation and neurodegeneration are delineated remains controversial (22).

Additionally, our study highlights structural remodeling within lesion regions, particularly around the BBB. Reduced continuity of CD31+ endothelial cells and the increased proximity of Claudin-5+ cells to BAX+ apoptotic cells suggest that EBV may contribute to vascular damage and compromise BBB integrity. This structural instability is especially evident in SPMS, where Claudin-5+ endothelial cells are more closely associated with astrocytic markers like Glut-1. These BBB disruptions could facilitate immune cell infiltration into the CNS, perpetuating the inflammatory cycle typical of MS.

Our study illuminates the significant role of EBV in shaping the immune microenvironment within MS lesions, yet certain limitations warrant acknowledgment. While the spatial proximity of EBV-positive cells to immune, glial, and neuronal populations—observed both through analysis and visually in stained tissue—provides compelling evidence of cellular relationships within MS lesions, direct confirmation of interactions will be one of the next steps in this analysis. Demonstrating ligand–receptor interactions would be useful to validate these putative encounters and elucidate molecular pathways. To further validate the specificity of our EBNA1 staining, we demonstrated its presence in EBV-infected tonsils, a well-characterized control tissue for EBV localization. The resulting images, along with EBER-ISH findings, confirmed EBNA1 staining in both the nucleus and cytoplasm, providing strong evidence for the accuracy of our staining approach. This validation reinforces the reliability of our observations and supports the conclusion that the identified EBV markers represent true viral presence rather than nonspecific staining artifacts.

Although our small cohort size limits generalizability, the consistency of findings across two independent biobanks strengthens the robustness of our conclusions. By visualizing the proximity of EBV-positive cells to glial and neuronal populations in situ, this study offers a biologically meaningful proxy for potential cellular interactions, providing insights into how EBV may influence neuroinflammation and tissue damage. Future work will expand cohort sizes and explore receptor–ligand mechanisms to build on these findings and advance our understanding of EBV's role in MS pathology and therapeutic potential.

The findings of this study underscore the potential of targeting EBV as a focus for future therapies for MS. Antiviral therapies or immune modulation targeting EBV within the CNS could mitigate lesion formation and limit disease progression. Future studies should explore the efficacy of treatments specifically addressing EBV's role in CNS immune activation and BBB disruption as part of a comprehensive strategy to manage MS.

Materials and Methods

Cohort Description and Sample Collection. This study includes postmortem brain tissue samples from patients diagnosed with MS, including subtypes such as PPMS and SPMS, as well as matched non-MS controls. These samples were obtained from the Maritime Brain Tissue Biobank (<https://www.mbtb.ca>) and the Netherlands Brain Bank (<https://www.brainbank.nl>). MS tissue samples from the Maritime Brain Tissue Biobank overlap with specimens previously analyzed in ref. 7, where increased frequencies of EBV-positive B cells expressing LMP1, BZLF1, and/or EBER were identified, allowing for complementary insights into EBV's role in the MS lesion microenvironment.

In this study, we reanalyzed these shared specimens using advanced multiplexed histological tools to gain enhanced spatial resolution and investigate EBV-positive cells' interactions with neighboring cellular populations. *SI Appendix, Fig. S1B* highlights the EBER staining performed on these specimens during Moreno et al., which validates the presence of EBV markers in this cohort. To complement these analyses, we incorporated an additional set of samples from the Netherlands Brain Bank, broadening the scope of our findings and assessing their generalizability. However, EBER staining has not yet been performed on this new cohort, marking an avenue for future investigation. Fifteen samples were included in the study, with a diversity in age (47 to 86 y) and gender representation. Each MS sample is paired with a control to mitigate age-related confounders. *SI Appendix, Table S2* describes the full details of the specimens utilized for this study.

Sample Preparation for AKOYA PhenoCycler Imaging. Formalin-fixed, paraffin-embedded (FFPE) brain tissue was sectioned at 5 μm , mounted on Poly-L-Lysine glass slides, and stained with hematoxylin and eosin (H&E) prior to multiplexed imaging using Akoya's PhenoCycler-Fusion system. This high-dimensional tissue profiling technique enables the spatial resolution of 42 markers, including EBV-associated markers (EBNA1 and LMP1), immune markers (CD4, CD8, IBA1, and CD20), neuroglial (GFAP, Olig2, and Neun), structural (CollagenIV), and metabolic markers (BAX, BCL-XL, and Ki67). A full description of the panel, staining conditions, as well as marker combinations used to identify cells, is found in *SI Appendix, Tables S3–S5*.

Antibody Panel and Staining Protocol. The antibody panel assessed immune cells, glial cells, vascular cells, and EBV-related markers. *SI Appendix, Table S3* describes the panel calibrated for these experiments. Notable antibodies include EBV markers (EBNA1, LMP1, and EBNA2), immune markers (CD4, CD8, IBA1, and CD20), glial markers (GFAP for astrocytes and Olig2 for oligodendrocytes), and endothelial markers (CD31).

Multiplexed Imaging and Spatial Analysis Workflow. Multiplexed imaging was performed using the PhenoCycler-Fusion 2.0 system (Akoya Biosciences, PhenoCycler-Fusion), enabling the visualization of up to 42 markers within a single tissue section. FFPE tissue sections were first stained with a panel of antibodies conjugated to DNA barcodes, allowing for iterative imaging. During each imaging cycle, antibodies specific to a subset of markers were applied, followed by fluorescence imaging to capture marker localization. The barcoded antibodies were then stripped, and a new set of antibodies was introduced for subsequent cycles. This iterative process ensured comprehensive, high-dimensional profiling while preserving tissue integrity. High-resolution images were acquired at each step, capturing cellular and subcellular localization of markers.

Data analysis was conducted using the Enable Medicine Analysis Platform (Enable Medicine Inc.), which supports advanced multiplexed imaging workflows. Images were preprocessed to normalize intensity, and cell segmentation was performed using deep-learning-based algorithms, such as the Mesmer model, which delineates nuclear and cytoplasmic boundaries. Quantitative data on biomarker expression and spatial coordinates were extracted for each segmented cell. Regions of interest (ROIs), including lesions and areas with compromised BBB integrity, were identified for focused analysis.

Spatial interactions were quantified using proximity and colocalization analyses. Proximity analysis involved calculating Euclidean distances between specific cell types, such as immune, glial, neuronal, and EBV-positive cells, to reveal shifts in cellular organization. Colocalization analysis employed log₂ odds ratios to assess the likelihood of marker overlap or adjacency, highlighting areas with enriched interactions. The analysis provided granular insights into immune–glial–neuronal relationships and the spatial distribution of EBV-positive cells within lesions. These methods facilitated the detailed mapping of cellular interactions and BBB disruptions, uncovering key alterations in the microenvironment of MS lesions.

Cell Segmentation. Cell segmentation is the process of identifying and delineating individual cells within an image, typically using computational methods, to analyze their morphology, location, and interactions in biological studies. Cell segmentation was performed using DeepCell, a deep learning-based segmentation model developed by the Van Valen Lab at Caltech and the Angelo Lab at Stanford. The model, based on the *Mesmer* algorithm (DeepCell version 0.12.6), was trained on TissueNet, a large image dataset containing over 1 million paired whole-cell and nuclear annotations. Input to the model included a nuclear biomarker and, optionally, a cytoplasmic or membrane biomarker to segment whole cells. Segmentation enabled accurate identification of individual cells within the tissue, allowing for the quantification of biomarker intensity within the cell boundaries for downstream analysis.

Gating Cell Populations. Cell populations of interest (immune, glial, neuronal, and EBV-positive cells) were identified and isolated using manual and automated gating approaches. Manual gating was first performed by adjusting marker intensity thresholds to define cell populations (e.g., CD4, CD8 for immune cells, GFAP for astrocytes, EBNA1 for EBV-positive cells). This step allowed for careful identification in complex tissue areas, particularly where marker overlaps occurred, ensuring accurate population classification.

Following this, automated gating was applied using the RESTORE algorithm (23), which classifies cells based on mutually exclusive biomarker pairs, normalizing background signals for improved accuracy. This method is beneficial for large datasets where manual gating is less practical, providing high reproducibility. Both methods included quality control steps: exclusion of cells with low marker expression, doublet exclusion using RESTORE, and visual validation to ensure proper cell identification.

ROIs. ROIs were defined to focus the analysis on specific areas of the tissue that were relevant to the study's hypotheses. ROIs were selected based on pathological features, such as lesion areas or regions with disrupted BBB integrity, which were expected to exhibit significant immune interactions and EBV-positive cell localization in MS tissue.

For each sample, ROIs were manually or semiautomatically identified on the tissue sections based on histological characteristics and the presence of key markers (e.g., EBV, CD4, CD8, GFAP, etc.). Once the ROIs were defined, the analysis focused exclusively on these regions, ensuring that cell-cell interactions and spatial proximity were quantified and relevant to the pathological context of MS lesions.

Spatial Neighbor Distance Analysis. Spatial relationships between immune, glial, and EBV-positive cells were quantified using the Spatial Neighbor Distance extension. For each cell of a given "from" cell type, the nearest neighbor of a different "to" cell type was identified, and the Euclidean distance between these cells was computed. The distances were then analyzed to assess the proximity of immune cells and glial cells to EBV-positive cells in MS and control tissue regions. Results were visualized in histograms, which displayed the distribution of cell-cell interaction distances for immune cells, glial cells, and EBV-positive cells. These histograms were generated using the Seaborn package in Python, with the density plot overlaid using the `seaborn.histplot` function and the `kde=True` argument to provide a smooth density estimate of the distribution. Separate histograms were generated for MS and control tissue regions to compare the spatial proximity of the cell types between the two groups.

Log2 Odds Ratio Calculation. The log₂ odds ratio (log₂ OR), as described by Goltsev et al. (8), was used to quantify the association and colocalization of different cell types within the tissue microenvironment. The log₂ OR was calculated to assess the likelihood of colocalization between two markers relative to their independent occurrences. The formula for calculating the log₂ OR is as follows:

$$\log_2 \text{OR} = \log_2 \left(\frac{P(\text{MarkerA} \cap \text{MarkerB})}{P(\text{MarkerA}) \times P(\text{MarkerB})} \right),$$

where $P(\text{MarkerA} \cap \text{MarkerB})$ represents the probability that both markers A and B colocalize at the same spatial location, and $P(\text{MarkerA})$ and $P(\text{MarkerB})$ represent the independent probabilities of each marker's presence in the tissue.

Interpretation of the log₂ OR:

A log₂ OR > 0 indicates that markers A and B are more likely to colocalize than expected by chance.

A log₂ OR < 0 suggests less colocalization than expected by chance.

A log₂ OR = 0 implies no significant colocalization, indicating independent presence of the markers.

Volcano plots were used to visualize the log-fold change (LFC) in feature abundance between two cohorts (x-axis) and the statistical significance (negative log₁₀ of *P*-value, y-axis). Positive LFC indicates enrichment, and negative LFC indicates depletion. Features with high statistical significance and large LFC are plotted toward the top and sides. Welch's *t* test was used to compare the means between two cohorts and assess statistical significance. This calculation was applied to assess the spatial interactions between immune cells, glial cells, and EBV-positive cells, providing insights into their relationships within MS lesions and control tissue.

ISH. ISH was performed on the same FFPE blocks used for CODEX to detect EBV RNA expression. The EBER-1 dinitrophenyl (DNP) probe was used to detect EBER-1 (ISH iView kit; Ventana Medical Systems Inc., Tucson, AZ, Cat# 760-097). EBER-ISH was performed using an automated Ventana BenchMark XT system (Ventana Inc.) in accordance with the manufacturer's protocol. Briefly, FFPE sections were treated with EZ Prep buffer (Ventana Inc.) to remove paraffin, rehydrated, and then digested with ISH protease 1 (Ventana Inc., Cat# 780-4147). The EBER-1 DNP probe was hybridized to the target RNA, followed by stringency washes as per the manufacturer's instructions using SSC buffer (Ventana Inc., Cat# 950-110). Slides were counterstained with Red Counterstain II (Ventana Inc., Cat# 780-2218) for visualization. Serial sections of all samples were also stained with oligo-T probes to confirm RNA preservation in each sample. EBV-infected tonsil tissue from a case of infectious mononucleosis was used as a positive control, while tonsil tissue from a healthy individual served as a negative control. EBER-ISH findings were used to validate EBV RNA presence in MS lesions, demonstrating both nuclear and some cytoplasmic localization.

Statistical Analysis. Statistical analyses were performed using the tools available within the Enable Medicine platform. To compare immune cell densities and spatial interactions between MS and control tissue samples, nonparametric tests (Mann-Whitney *U* test) were applied. In volcano plots and box plots (scatter plots), Welch's *t* test was used to compare the means between two cohorts, determining whether the observed differences were statistically significant. *P*-values < 0.05 were considered statistically significant. All analyses were performed without post hoc correction methods (e.g., Bonferroni or Benjamini-Hochberg), as the primary focus was on direct group comparisons without multiple testing adjustments.

Data Visualization and Summary. Data were visualized using the Enable Medicine platform's integrated tools, which generated high-dimensional maps and heatmaps of cell localization and interactions. The platform also provided summary statistics of the spatial distances between cell types, including the mean, median, SD, minimum, and maximum distances. These summaries were used to compare MS and control tissue regions, identifying significant differences in the proximity of immune and glial cells to EBV-positive cells.

Data, Materials, and Software Availability. The datasets and images generated and analyzed in this study are publicly available in the Stanford Digital Repository (SDR) (24). The analysis for this study was conducted using the Enable Medicine Analysis Platform (Enable Medicine Inc.), a proprietary software designed for high-dimensional imaging and spatial analysis of multiplexed tissue profiles. This platform enables the processing, segmentation, and visualization of complex tissue interactions. Information regarding its capabilities can be found on the Enable Medicine website (<https://www.enablemedicine.com/platform>) (25). All other data are included in the article and/or *SI Appendix*.

ACKNOWLEDGMENTS. This research project was funded by F. Hoffmann-La Roche Ltd., Basel, Switzerland, as part of the Integrative Neuroscience Collaborations Network. We want to extend our sincere gratitude to Dr. Rosetta Pedotti, Dr. Catarina Raposo, and Dr. Bjoern Tackenberg for their invaluable input on the project and their contributions to the preparation of this manuscript. Their expertise and support have been instrumental in advancing this work.

Author affiliations: ^aDepartment of Neurology and Neurological Sciences, Stanford University, Stanford, CA 94305-5316; and ^bDepartment of Pediatrics, Stanford University, Stanford, CA 94305-5316

1. S. S. Soldan, P. M. Lieberman, Epstein-Barr virus and multiple sclerosis. *Nat. Rev. Microbiol.* **21**, 51–64 (2023).
2. T. V. Lanz *et al.*, Clonally expanded B cells in multiple sclerosis bind EBV EBNA1 and GlialCAM. *Nature* **603**, 321–327 (2022).
3. F. Aloisi, M. Salvetti, EBV infection drives MS pathology: Yes. *Mult. Scler.* **30**, 483–485 (2024).
4. K. Bjornevik, C. Münz, J. I. Cohen, A. Ascherio, Epstein-Barr virus as a leading cause of multiple sclerosis: Mechanisms and implications. *Nat. Rev. Neurol.* **19**, 160–171 (2023), <https://doi.org/10.1038/s41582-023-00775-5>.
5. W. H. Robinson, L. Steinman, Epstein-Barr virus and multiple sclerosis. *Science* **375**, 264–265 (2022).
6. T. V. Lanz, W. H. Robinson, P. P. Ho, L. Steinman, Roadmap for understanding mechanisms on how Epstein-Barr virus triggers multiple sclerosis and for translating these discoveries in clinical trials. *Clin. Transl. Immunol.* **12**, e1438 (2023).
7. M. A. Moreno *et al.*, Molecular signature of Epstein-Barr virus infection in MS brain lesions. *Neuroimmunol. Neuroinflamm.* **5**, e466 (2018).
8. Y. Goltsev *et al.*, Deep profiling of mouse splenic architecture with CODEX multiplexed imaging. *Cell* **174**, 968–981.e15 (2018).
9. V. E. Miron *et al.*, M2 microglia and macrophages drive oligodendrocyte differentiation during CNS remyelination. *Nat. Neurosci.* **16**, 1211–1218 (2013).
10. C. S. Leung, T. A. Haigh, L. K. Mackay, A. B. Rickinson, G. S. Taylor, Nuclear location of an endogenously expressed antigen, EBNA1, restricts access to macroautophagy and the range of CD4 epitope display. *Proc. Natl. Acad. Sci. U.S.A.* **107**, 2165–2170 (2010).
11. M.-S. Kang *et al.*, Roscovitine inhibits EBNA1 serine 393 phosphorylation, nuclear localization, transcription, and episome maintenance. *J. Virol.* **85**, 2859–2868 (2011).
12. A. Hassani, J. R. Corboy, S. Al-Salam, G. Khan, Epstein-Barr virus is present in the brain of most cases of multiple sclerosis and may engage more than just B cells. *PLoS One* **13**, e0192109 (2018).
13. H. C. Jha *et al.*, Gammaherpesvirus infection of human neuronal cells. *mBio* **6**, e01844–15 (2015).
14. A. Menet *et al.*, Epstein-Barr virus infection of human astrocyte cell lines. *J. Virol.* **73**, 7722 (1999).
15. A. Biebl *et al.*, Fatal Epstein-Barr virus encephalitis in a 12-year-old child: An underappreciated neurological complication? *Nat. Rev. Neurol.* **5**, 171–174 (2009).
16. D. Tiwari, N. Mittal, H. C. Jha, Unraveling the links between neurodegeneration and Epstein-Barr virus-mediated cell cycle dysregulation. *Curr. Res. Neurobiol.* **3**, 100046 (2022).
17. B. Serafini, L. Benincasa, B. Rosicarelli, F. Aloisi, EBV infected cells in the multiple sclerosis brain express PD-L1: How the virus and its niche may escape immune surveillance. *J. Neuroimmunol.* **389**, 578314 (2024).
18. S. S. Ousman *et al.*, Protective and therapeutic role for α B-crystallin in autoimmune demyelination. *Nature* **448**, 474–479 (2007).
19. R. M. Ransohoff, Assault on the guardian. *Nature* **448**, 421–422 (2007).
20. O. G. Thomas *et al.*, Cross-reactive EBNA1 immunity targets alpha-crystallin B and is associated with multiple sclerosis. *Sci. Adv.* **9**, eadg3032 (2023).
21. N. Sattarnejad, I. Kockum, L. Steinman, W. H. Robinson, T. V. Lanz, Antibody reactivity against EBNA1 and GlialCAM differentiates multiple sclerosis patients from healthy controls. *Proc. Natl. Acad. Sci. U.S.A.*, in press.
22. L. Steinman, S. S. Zamvil, Beginning of the end of two-stage theory purporting that inflammation then degeneration explains pathogenesis of progressive multiple sclerosis. *Curr. Opin. Neurol.* **29**, 340–344 (2016).
23. Y. H. Chang *et al.*, RESTORE: Robust intEnSiTy nORmalization mEthod for multiplexed imaging. *Commun. Biol.* **3**, 111 (2020).
24. N. Orr (Or-Geva), L. Steinman, Epstein-Barr virus and the immune microenvironment in multiple sclerosis: Insights from high-dimensional brain tissue imaging. Version 1. Stanford Digital Repository. <https://purl.stanford.edu/rd004fn9297>. Deposited 25 February 2025.
25. Enable Medicine Platform, Enable Atlas. <https://www.enablemedicine.com/platform>. Accessed 29 August 2024.